Anomalous Behavior of Proton Zero Point Motion in Water Confined in Carbon Nanotubes

G. Reiter,[1] C. Burnham,[1] D. Homouz,[1] P. M. Platzman,[2] J. Mayers,[3] T. Abdul-Redah,[3] A. P. Moravsky,[4] J. C. Li,[5] C.-K. Loong,[6] and A. I. Kolesnikov[6]

[1]*Physics Department, University of Houston, 4800 Calhoun Road, Houston, Texas 77204, USA*
[2]*Bell Labs, 600 Mountain Avenue, Murray Hill, New Jersey 07974, USA*
[3]*ISIS Facility, Rutherford Appleton Laboratory, Chilton, Didcot, Oxfordshire, OX11 0QX, United Kingdom*
[4]*MER Corporation, 7960 South Kolb Road, Tucson, Arizona 85706, USA*
[5]*Department of Physics, UMIST, P.O. Box 88, Manchester, M60 1QD, United Kingdom*
[6]*Intense Pulsed Neutron Source, Argonne National Laboratory, South Cass Avenue, Argonne, Illinois 60439, USA*

(Received 4 January 2006; published 14 December 2006)

The momentum distribution of the protons in ice I_h, ice VI, high density amorphous ice, and water in carbon nanotubes has been measured using deep inelastic neutron scattering. We find that at 5 K the kinetic energy of the protons is 35 meV less than that in ice I_h at the same temperature, and the high momentum tail of the distribution, characteristic of the molecular covalent bond, is not present. We observe a phase transition between 230 and 268 K to a phase that does resemble ice I_h. Although there is yet no model for water that explains the low temperature momentum distribution, our data reveal that the protons in the hydrogen bonds are coherently delocalized and that the low temperature phase is a qualitatively new phase of ice.

DOI: 10.1103/PhysRevLett.97.247801 PACS numbers: 61.25.Em

Water in carbon nanotubes is of interest as a model system for the study of water in quasi-one-dimensional confined spaces [1], where otherwise inaccessible liquid and glassy phases exist over a wide range of temperatures. It has possible applications to nanotechnology [2,3] and the understanding of transport in biological pores [4–6]. There is a consensus, arising from simulations of the structure, that, for sufficiently large nanotubes, the water entering initially forms an ordered 2D square ice layer lining the nanotube [4,7,8]. The momentum distribution of the protons, which, at the temperature of the measurements, is due almost entirely to zero point motion, is a direct reflection of the structure of their local environment. It can be measured by deep inelastic neutron scattering (DINS), also called neutron Compton scattering [9–12]. We find from these measurements that the protons in nanotube water are in a unique quantum state, qualitatively different from that of protons in the other phases of ice that we have measured: ice I_h, ice VI, and high density amorphous (HDA) ice. The kinetic energy of the protons is 35 meV less than that of the protons in ice I_h at the same temperature, and the high momentum tail, characteristic of the molecular covalent bond and the stretch mode in the water molecule, is missing. There is a transition between 230 and 268 K to a 3D coordinated state that resembles the other phases of ice in the value of its kinetic energy and the presence of a high momentum tail in the momentum distribution. This is above the value (200 K) predicted by our simulations of the structure, which are, however, classical and do not satisfactorily include the quantum effects discussed here.

DINS is inelastic neutron scattering in the limit of large momentum transfer $\vec{q}$ (30–100 Å^{-1}). In this limit, the neutrons scatter from the individual protons in the same manner that freely moving particles scatter from each other. The fraction of neutrons scattered into a given angle with a given energy depends only on the probability that the proton had a particular momentum at the time it was struck by the neutron $n(\vec{p})$. There is scattering of the neutrons off of the other ions as well, with the center of the peak due to an ion of mass M located at an energy of $\hbar^2 q^2/2M$. Because of the much heavier mass of the carbon and oxygen, this scattering is easily separated from that of the protons. We actually measure directly the usual neutron scattering function $S(\vec{q}, \omega)$, which in the limit of large momentum transfer, and for a randomly oriented powder sample such as ours, has the impulse approximation form [9]

$$S_{\mathrm{IA}}(\mathbf{q}, \omega) = \frac{M}{q} J(y) = \frac{M}{q} \int n(p) \delta(y - \vec{p} \cdot \hat{q}) d\mathbf{p}, \quad (1)$$

where $y = \frac{M}{q}[\omega - (\hbar q^2/2M)]$ and $\hat{q}$ is a unit vector in the direction of the momentum transfer.

The momentum distribution $n(p)$ can be extracted from the measurements in a manner described in detail in earlier work [9,10,12]. $S_{\mathrm{IA}}(\mathbf{q}, \omega)$ is represented as a series expansion in Hermite polynomials. Small corrections due to deviations from the impulse approximation are added, the total is convolved with the instrumental resolution function, and the coefficients in the series expansion determined by a least squares fitting procedure.

$n(p)$ is then given by the expansion

$$n(p) = \frac{e^{-\frac{p^2}{2\sigma^2}}}{(\sqrt{2\pi}\sigma)^3} \sum_{n=0}^{\infty} a_n (-1)^n L_n^{1/2}\left(\frac{p^2}{2\sigma^2}\right), \quad (2)$$

where the $L_n^{1/2}(p^2/2\sigma^2)$ are associated Laguerre polynomials, and the a_n are arbitrary coefficients to be determined by the least square fitting process [13] $a_0 = 1$. Terms with

$n > 5$ are not statistically significant in these experiments. The parameter σ that determines the width of the momentum distribution is related to the kinetic energy of the proton by $E_{\mathrm{kin}} = 6.27\sigma^2$ when σ is expressed in inverse angstroms and the kinetic energy in meV, independently of any of the remaining coefficients if the term with $n = 1$ is omitted in Eq. (2) [12]. The errors in the measured momentum distribution are related to the uncertainties in the coefficients in the expansion [10], which are obtained from the least squares fitting program, making a point by point calculation of the probable error possible.

The experiments were all done on the VESUVIO instrument at ISIS. There were 28 detectors in all, arranged symmetrically around the beam, with scattering angles from 35°–67°. The 3 g sample of opened single walled carbon nanotubes (SWNTs) 14 ± 1 Å diameter and about 10 μm in length [14] was used for DINS measurements. To fill nanotubes with water, the dry SWNT sample was first exposed in water vapor at 110 °C for 2 h in an enclosed environment. The excess water adsorbed in the exterior of the nanotubes was then extracted by evaporation at 45 °C to the final H_2O-to-SWNT mass ratio of about 11.5 wt %. High-pressure phase ice VI and HDA ice were prepared from double distilled H_2O water by pressurizing the initial hexagonal ice I_h in a piston-cylinder pressure cell to 15 kbar, at about 270 K temperature for ice VI and at 77 K for HDA ice. The ice VI sample was then cooled to 77 K at 15 kbar. The pressure was released, and both samples were then recovered at the low temperature ($T =$ 77 K).

We show in Fig. 1 the signal for the Compton profile $J(y)$ obtained directly from the data by adding the signal that comes from intervals of time for each detector that map into an interval Δy, there being 100 such Δy intervals in all. The average over all detectors can be done as there is

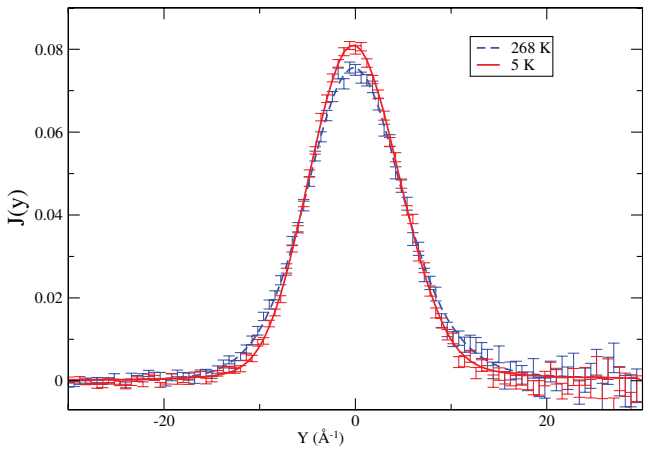

FIG. 1 (color online). The experimental neutron Compton profile $J(y)$ at 5 and 268 K, constructed by binning the time of flight data for each of the 28 detectors in Δy bins assuming that the data satisfies y scaling [Eq. (1)]. The solid and dashed curves are fits to the entire data set and include the instrumental resolution and final state effects.

no significant variation with detector angle of the signal in the data. There is some systematic distortion that arises from binning in this way, as the Sears final state corrections [15] to the impulse approximation do not obey y scaling, and the binning procedure itself introduces some discreteness noise. The signal shown in Fig. 1 includes the instrumental resolution. Nevertheless, it is clear to the eye that the 5 K data are considerably narrower than those at 268 K. The proper way to fit the entire data set is with the polynomial expansion, as described above. The parameters characterizing the fits are shown in Table I, along with those for the other samples we have measured [16].

We show in Fig. 2 a comparison of the fitted radial momentum distributions $[4\pi p^2 n(p)]$ for the water in the nanotubes at 5 K with bulk polycrystalline ice I_h, ice VI, and HDA ice, all at comparable temperatures. While there are significant differences between the various forms of ice, the water in the nanotubes, presumably also a form of ice at 5 K, is in a state that is qualitatively different from that of the others. This shows up dramatically in the narrowness of the momentum distribution. We find from Table I that the kinetic energy of a proton in the nanotube water is 35 meV less than that in ice I_h and 44 meV less than that in the 268 K phase.

Another difference that is indicative of a major change in the local structure is the absence of a broad high momentum tail in the nanotube data. Since the stretch mode due to motion along the bond is at a much higher frequency than the transverse modes (bending, libration), the momentum distribution will be much broader in the bond direction. When the individual molecule distribution is spherically averaged, the shape of the resulting curve at the momentum high compared to the transverse widths is determined entirely by the motion along the bond. This is shown in detail in the inset in Fig. 2, where an isotropically averaged momentum distribution is shown for several values of the transverse momentum widths.

The forms of bulk ice are similar at high momenta because the covalent bond of the proton to its molecular oxygen is similar, and this is the dominant interaction determining the stretch mode frequency. The absence of a high momentum tail, or rather its large reduction in intensity in the nanotube ice, indicates that the local structure of the water in nanotube ice is very different from that of the other forms of ice. A best fit with an anisotropic Gaussian distribution gives the widths along the bond and perpendicular to it as nearly equal and approximately 4 $\mathrm{Å}^{-1}$. The strong covalent molecular bond, responsible for the high frequency of the stretch mode in the harmonic approximation, with a momentum width of approximately 6 $\mathrm{Å}^{-1}$, appears to be missing.

According to simulations, the initial water molecules entering the nanotube form a 2D square ice sheath concentric with the walls of the nanotube [4,7,8]. The carbon nanotubes used here are sufficiently large (14 Å) that a chain of water molecules can fit down the center, in addi-

TABLE I. Parameters for fit.

Water sample	σ(Å^{-1})	a_2	a_3	a_4	a_5
Nanotube 5 K	4.11	-0.053 ± 0.013	0.041 ± 0.008	0.0	-0.053 ± 0.03
Ice I_h 5 K	4.79	0.018 ± 0.002	-0.028 ± 0.003	0.035 ± 0.004	-0.037 ± 0.004
HDA ice 5 K	4.74	0.0	0.0	0.051 ± 0.006	-0.054 ± 0.007
Ice VI 8 K	4.66	-0.019 ± 0.005	-0.0067 ± 0.003	0.035 ± 0.004	-0.057 ± 0.009
Nanotube 268 K	4.82	0.067 ± 0.010	-0.078 ± 0.012	0.0	0.0

tion to the ice layer [8]. The absence of a high momentum tail in the momentum distribution must be a property of the ice sheath, perhaps in conjunction with the central molecules, since the sheath constitutes roughly 85% of the molecules.

Measurements at higher temperatures provide further evidence that the anomalous quantum state is associated with the 2D ice sheath. We have made DINS measurements of nanotube water at 170 and 230 K as well. These are indistinguishable, within the experimental uncertainty, from those at 5 K. However, the distribution at 268 K, shown in Fig. 3, is dramatically different and has the high momentum tail that we associate with the stretch modes in the harmonic approximation. Evidently, the local structure around the proton has changed. The molecular dynamics (MD) simulations also show a change in the global structure of the water in the nanotubes above 200 K, from a two-dimensional cylindrical ice sheath and chain to a three-dimensionally hydrogen bonded structure that resembles bulk water or ice. The existence of the phase change is in agreement with earlier work [7,17] and more recent measurements [18]. We show also in Fig. 3 a fit to the data (circles) obtained from a simple model in which the wave function along the bond direction is the sum of two Gaussians displaced a distance d. The distribution perpendicular to the bond is taken to be a Gaussian, with the two directions equivalent. The potential along the bond that would lead to such a wave function and the wave function itself are shown in the inset in Fig. 3. The fitted value for the separation d is 0.21 Å. σ_z, the momentum width in the absence of any separation, is 5.81 Å^{-1}, and the transverse momentum distribution widths are 4.16 Å^{-1}. We note that this separation is consistent with the low temperature Debye Waller measurements of Ref. [8]. However, the flat potential that was hypothesized to explain those results was taken to be in the transverse direction to the hydrogen bonds of the chain. We see here that it is the motion along the bond that is enhanced, and that is so for nearly all of the molecules. Furthermore, since the momentum distribution narrows, the large Debye Waller factor cannot be due to

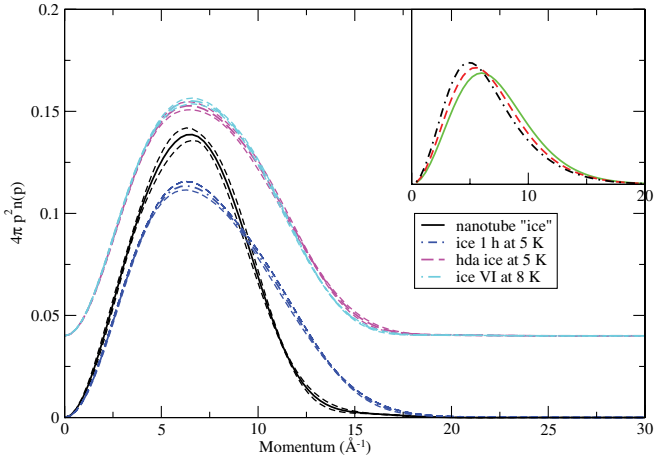

FIG. 2 (color online). The momentum distribution of the protons in nanotube ice compared with that in three forms of bulk ice. The dotted lines are 1 standard deviation error limits. The inset shows the effect of varying the parameters in an anisotropic harmonic model of the proton momentum distribution in the hydrogen bond, with the momentum width along the bond fixed and the transverse widths varied [2.8 (dotted-dashed curve), 3.2 (dashed curve), and 3.6 Å^{-1} (solid curve)], keeping the width along the bond of 6 Å^{-1}. The lowest value of the transverse width gives a kinetic energy comparable to that observed in the nanotubes at 5 K; the highest value corresponds to the fit to the ice I_h data [12]. The HDA ice and ice VI data are displaced vertically for clarity.

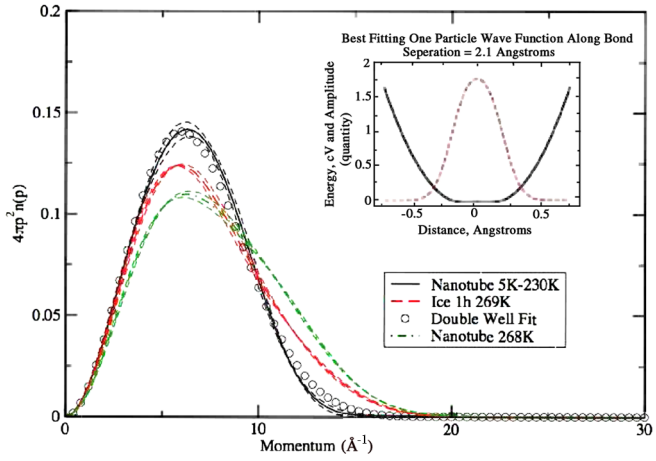

FIG. 3 (color online). Comparison of the momentum distributions for nanotube ice at 268 K, bulk ice I_h at 269 K, and the low temperature phase of nanotube ice, represented by the data at 5 K. The circles are a fit to a model in which the proton is delocalized along the bond in a double well potential. The potential (solid curve) and the wave function (dashed curve) corresponding to the fit to the momentum distribution data along the bond direction are shown in the inset.

statistical disorder in the position of the proton but must reflect a coherent delocalization.

The coherent delocalization that we are seeing in the wave function and the flat bottom of the well could be the result of interactions between the protons, perhaps involving the central chain molecules, which do form temporary weak H bonds with the ice layer. Indeed, a purely one-particle interpretation that regards the stretch frequency as due to the motion of the proton in a fixed potential formed by the oxygens cannot simultaneously explain the narrow momentum distribution and the slight increase in the stretch mode frequency observed in INS [8]. The potential in Fig. 3 should then be regarded as an effective mean field potential. We cannot, however, propose a convincing many-body interpretation at this time.

Numerous previous measurements on VESUVIO have indicated the existence of an intensity deficit in scattering from hydrogen [19]. There are competing theories of these anomalies: those based on the symmetry under particle interchange of the many-particle proton wave function [20], which predict a reduction of the scattered intensity with no distortion of the shape of the measured Compton profile, and those based on Born-Oppenheimer breakdown [21,22]. The intermediate coupling regime of one of these theories [21], appropriate for a large, q-independent, intensity deficit such as observed in bulk water, predicts that such distortions could occur. If the distortions were large enough, the data for the summation of all the detectors, shown in Fig. 1, would not collapse to a single curve [23]. The absence of a distortion of the Compton profile indicated by the data collapse could be inconsistent, therefore, with the Born-Oppenheimer breakdown mechanism for the deficit. Since (within experimental error) data collapse is observed at both temperatures, the Born-Oppenheimer breakdown mechanism either is not applicable or does not distort the Compton profile significantly. In either case, it cannot be responsible for the difference with temperature seen in Fig. 1.

Whatever the explanation, it is clear that the quantum state of the protons in the low temperature phase of water in these nanotubes is qualitatively different from that of any phase of water seen so far. The transition temperature to a normal bulk water/icelike phase is likely to be dependent on the size of the nanotube and the details of the interaction of the water molecules with the confining cylinder [4]. Should the phase exist at room temperatures in different size cylinders, its properties would be of great interest in understanding the structure and transport of water in biological pores.

The work at Argonne National Laboratory was supported by the Office of Basic Energy Sciences, Division of Materials Sciences, U.S. Department of Energy, under Contract No. W-31-109-ENG-38. C. B. is thankful for a grant from Argonne Theory Institute for his stay at IPNS. The MD calculations were made with a grant of time on the Argonne National Laboratory Jazz computer. The work of G. R., C. B., D. H., and P. M. P. was supported by DOE Grant No. DE-FG02-03ER46078.

[1] G. Hummer, J. C. Rasaiah, and J. P. Noworyta, Nature (London) **414**, 188 (2001).
[2] P. M. Ajayan, O. Stephan, P. Redlich, and C. Colliex, Nature (London) **375**, 564 (1995).
[3] R. R. Meyer *et al.*, Science **289**, 1324 (2000).
[4] W. H. Noon, K. D. Ausman, R. E. Smalley, and J. Ma, Chem. Phys. Lett. **355**, 445 (2002).
[5] A. Kaira, S. Garde, and G. Hummer, Proc. Natl. Acad. Sci. U.S.A. **100**, 10 175 (2003).
[6] M. Majumdar, N. Chopra, R. Andrews, and B. J. Hinds, Nature (London) **438**, 44 (2005).
[7] K. Koga, G. T. Gao, H. Tanaka, and X. C. Zeng, Nature (London) **412**, 802 (2001).
[8] A. I. Kolesnikov *et al.*, Phys. Rev. Lett. **93**, 035503 (2004).
[9] G. Reiter and R. Silver, Phys. Rev. Lett. **54**, 1047 (1985).
[10] G. F. Reiter, J. Mayers, and J. Noreland, Phys. Rev. B **65**, 104305 (2002).
[11] G. F. Reiter, J. Mayers, and P. Platzman, Phys. Rev. Lett. **89**, 135505 (2002).
[12] G. Reiter *et al.*, Braz. J. Phys. **34**, 142 (2004).
[13] The normalization of the coefficients is consistent with Ref. [12] and differs from that in Ref. [10].
[14] The samples were those used in Ref. [8]. The length was stated incorrectly there as 10 nm.
[15] V. F. Sears, Phys. Rev. **185**, 200 (1969); Phys. Rev. A **7**, 340 (1973).
[16] The parameter σ is a scale parameter in the final fit and so does not have error bars associated with it. This parameter is typically uncertain to 0.5% if it is regarded as a fitting parameter.
[17] Y. Maniwa *et al.*, J. Phys. Soc. Jpn. **71**, 2863 (2002).
[18] E. Mamontov *et al.*, J. Chem. Phys. **124**, 194703 (2006).
[19] C. A. Chatzidimitriou-Dreismann, T. Abdul Redah, R. M. F. Streffer, and J. Mayers, Phys. Rev. Lett. **79**, 2839 (1997); J. Mayers and T. Abdul-Redah, J. Phys. Condens. Matter **16**, 4811 (2004).
[20] E. B. Karlsson and S. W. Lovesey, Phys. Rev. A **61**, 062714 (2000); E. B. Karlsson and S. W. Lovesey, Phys. Scr. **65**, 112 (2002); H. Sugimoto, H. Yuuki, and A. Okumura, Phys. Rev. Lett. **94**, 165506 (2005).
[21] G. F. Reiter and P. M. Platzman, Phys. Rev. B **71**, 054107 (2005); D. Colognesi, Physica (Amsterdam) **358B**, 114 (2005).
[22] N. I. Gidopoulos, Phys. Rev. B **71**, 054106 (2005).
[23] The data for each detector have been fit with a single $J(y)$ given by Eqs. (1) and (2), including the final state corrections. Any systematic distortions would show up as systematic variations in the chi-squared values with angle, which we do not see. See EPAPS Document No. E-PRLTAO-97-005651 for fits with the angle and the chi-squared value given on each plot. For more information on EPAPS, see http://www.aip.org/pubservs/epaps.html.